Structural disorder in AgBr on the approach to melting

1990 J. Phys.: Condens. Matter 2 2773

(http://iopscience.iop.org/0953-8984/2/12/002)

J. Phys.: Condens. Matter 2 (1990) 2773–2786. Printed in the UK

Structural disorder in AgBr on the approach to melting

D A Keen†, W Hayes and R L McGreevy
Clarendon Laboratory, Parks Road, Oxford OX1 3PU, UK

Received 20 October 1989

Abstract. The powder neutron diffraction pattern of AgBr has been measured at nine temperatures between 293 K and 703 K (melting point T_m = 701 K). The structure factors have been analysed using the reverse Monte Carlo modelling technique to produce three-dimensional distributions of ions which show the thermally induced structural disorder in AgBr. Anisotropic mean squared displacements about lattice sites and occupancy of interstitial $(\frac{1}{4}, \frac{1}{4}, \frac{1}{4})$ sites by Ag^+ ions have been calculated for each temperature, giving a quantitative description of the development of the structural disorder associated with pre-melting.

1. Introduction

The well known fast ion conductor AgI shows a large increase in ionic conductivity at T_c = 420 K associated with a first order phase transition. The structure changes from the low-temperature β phase (wurtzite) to the α phase, the latter having a body centred cubic arrangement of I^- ions and a liquid-like distribution of Ag^+ ions. The ionic conductivity increases by four orders of magnitude at T_c to $\sigma = 1.3\ \Omega^{-1}\ cm^{-1}$ and thereafter there is a slow increase with increasing temperature, reaching $\sigma = 2.6\ \Omega^{-1}\ cm^{-1}$ at the melting point (T_m = 825 K). Above T_m, σ actually decreases slightly (Börjesson and Torell 1987, Boyce and Huberman 1979).

The high temperature behaviour of both AgBr and AgCl is different from that of AgI. They retain a face-centred cubic (rocksalt) structure until melting (T_m = 701 K for AgBr and 728 K for AgCl), and the ionic conductivity shows a gradual increase with increasing temperature, attaining a value in AgBr of $\sigma \simeq 1\ \Omega^{-1}\ cm^{-1}$ just below T_m (Aboagye and Friauf 1975). Transport and thermal expansion measurements show the predominant thermally induced defect to be the cation Frenkel interstitial (Lawn 1963) although there is some evidence for anion Schottky defects (Batra and Slifkin 1976). It has been suggested that AgBr and AgCl have characteristics closer to those exhibited by the fluorite fast ion conductors than by AgI (Mellander and Lazarus 1984); fluorites are moderate Frenkel-type ionic conductors at low temperatures and become fast-ion conductors above a diffuse phase transition a few hundred degrees below melting (Hayes 1978). In both AgBr and AgCl the ionic conductivity increases faster with increasing temperature 100°–150° below T_m than would be expected on the basis of a temperature-independent Frenkel energy (Devlin and Corish 1987). Andreoni and Tosi (1983)

† Present address: Neutron Science Division, Rutherford Appleton Laboratory, Chilton, Didcot, Oxfordshire OX11 0QX, UK.

0953-8984/90/122773 + 14 $03.50

suggest that an increase in Schottky defects, producing lattice instability, precipitates melting before a fast ion transition can be reached in AgBr. Other mechanisms have been suggested to explain the high temperature conductivity anomaly, including temperature dependent contributions to the Frenkel energy and lattice softening (Aboagye and Friauf 1975, Lawn 1963, Devlin and Corish 1987). (For thorough reviews see Friauf (1984) and Hamilton (1988).) These results suggest that the term 'pre-melting', associated with structural disorder preceeding melting (Hayes 1986), may be appropriate to describe AgBr and AgCl.

It is clear that, for a full understanding of both the ionic conductivity and premelting in these materials, a more complete picture of the temperature dependent ionic disorder is needed. In the present study powder neutron diffraction from AgBr has been combined with reverse Monte Carlo analysis (McGreevy and Pusztai 1988) to provide information about the ionic processes responsible for pre-melting in AgBr as $T \rightarrow T_m$. It has been found that, although both the cations and the anions predominantly retain their lattice sites as temperature increases, the mean squared displacement of the Ag^+ ion becomes very anisotropic, the largest displacement being in the $\langle 111 \rangle$ direction. The occupancy of the $(\frac{1}{4}, \frac{1}{4}, \frac{1}{4})$ interstitial site is small and a peak in Ag^+ ion density at this position only occurs for values of $T_m - T < 15$ K.

2. Experimental details

Samples of AgBr were finely powdered and packed into thin-walled silica tubes of 10 mm diameter and sealed under vacuum. The powder neutron diffraction measurements were carried out on the D20 diffractometer at the Institut Laue–Langevin in Grenoble using an incident neutron wavelength of $\lambda_i = 0.94$ Å. A thermocouple was calibrated with respect to T_m by measuring the output in melting AgBr. With standard neutron furnace equipment and this thermocouple it was possible to measure to within $2° \pm 1°$ of T_m; the temperature uncertainty being due to the temperature gradient across the sample; the temperature stability was $\pm 0.2°$. Spectra were obtained at nine temperatures, 293, 490, 669, 684, 689, 697, 698, 699 and 703 K ($T_m = 701$ K). Each scan took approximately $2\frac{1}{2}$ hours and was repeated at each temperature to ensure no change in the spectrum due to slow changes in the sample (e.g. partial melting or recrystallisation). For background and absorption corrections and data normalisation the empty furnace was measured at 293 K, an empty container at 690 K and a vanadium bar at 293 K.

3. Analysis

The corrected and normalised structure factors, $F(Q)$, for all nine temperatures are shown in figure 1 where

$$F(Q) = c_+^2 \bar{b}_+^2 (A_{++}(Q) - 1) + c_-^2 \bar{b}_-^2 (A_{--}(Q) - 1) + 2c_+ c_- \bar{b}_+ \bar{b}_- (A_{+-}(Q) - 1) \tag{1}$$

c_i are the fractional atomic concentrations, $\bar{b}_i$ are the coherent neutron scattering lengths and $A_{ij}(Q)$ are the partial structure factors; + and − refer to the Ag^+ and Br^- ions respectively. There is considerable diffuse scattering even at room temperature and at elevated temperatures this is the dominant contribution to the structure factor, with

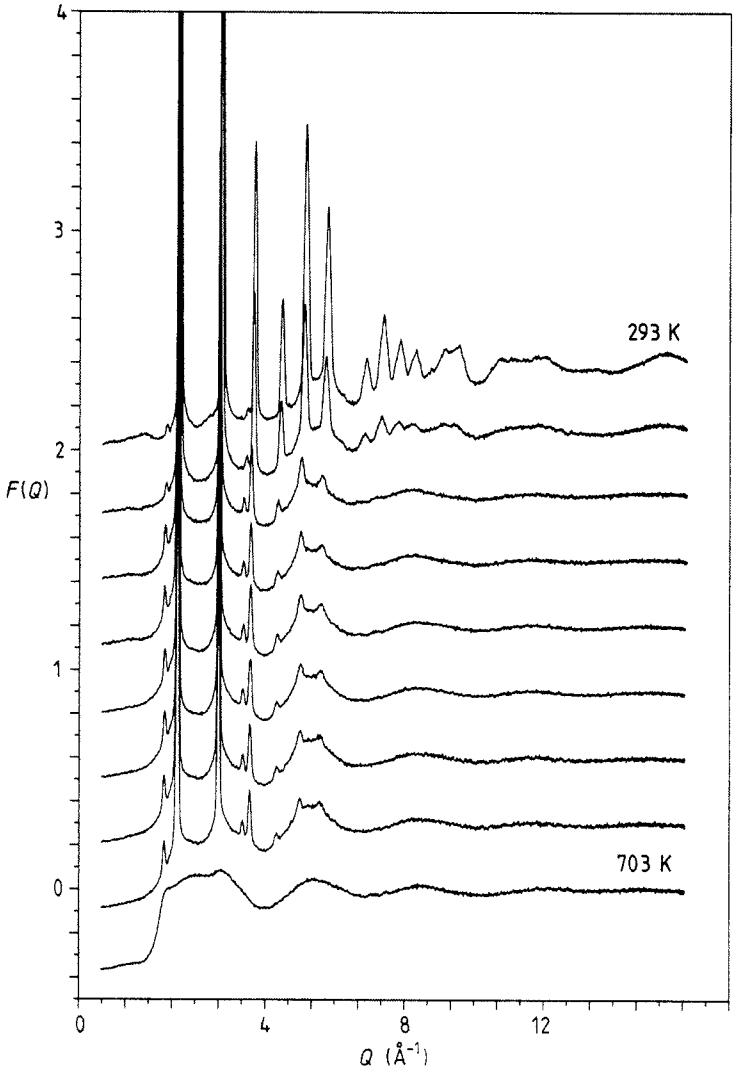

Figure 1. Structure factors of molten AgBr at 703 K and of AgBr powder at 699, 698, 697, 689, 684, 669, 490 and 293 K: each successive temperature has been offset vertically by 0.3. The (111) and (113) Bragg peaks are the first and fourth with increasing Q.

only a few Bragg peaks evident. The strongly Q dependent Bragg peak intensities suggest large thermal vibrations about lattice sites. For Bragg peaks where h, k, l are all odd, the rocksalt structure factor contains antiphase contributions from the cation and anion. The increase in intensity with increasing temperature of the (111) and (113) Bragg peaks therefore suggests that the ionic distributions about cation and anion lattice sites are changing relative to each other as the temperature is raised. Bragg peaks with h, k, l all even (in phase contributions) decrease in intensity as temperature increases.

The basic RMC modelling technique (McGreevy and Pusztai 1988) and its adaptation for analysis of powder spectra from disordered crystalline solids (Keen *et al* 1990) have been described elsewhere. It is a standard Metropolis Monte Carlo method (Metropolis

et al 1953) using a Markov chain convergence procedure. A configuration of M points in a cubic box of sides L with periodic boundary conditions is used to represent the ions in the crystal. After each particle move the radial distribution function $G_c(r)$ is calculated from the configuration and compared with $G_e(r)$, the experimental radial distribution function:

$$G(r) - 1 = [c_+^2 \bar{b}_+^2 (g_{++}(r) - 1) + c_-^2 \bar{b}_-^2 (g_{--}(r) - 1) + 2c_+ c_- \bar{b}_+ \bar{b}_- (g_{+-}(r) - 1)]/(c_+ \bar{b}_+ + c_- \bar{b}_-)^2 \quad (2)$$

where

$$g_{ij}(r) = \frac{1}{(2\pi)^3 \rho} \int 4\pi Q^2 (A_{ij}(Q) - 1) \frac{\sin(Qr)}{Qr} \, dQ$$

are the partial radial distribution functions and ρ is the number density of ions. Moves are accepted or rejected depending on the agreement between $G_c(r)$ and $G_e(r)$. This is assessed by calculating

$$\chi^2 = \frac{1}{2\sigma_e^2} \sum_{i=1}^{N} (G_c(r_i) - G_e(r_i))^2$$

where σ_e is an estimate of the experimental uncertainty and N is the number of r points in $G_e(r)$. $\chi^2 \equiv U/kT$ in the standard Monte Carlo method where U is the total potential energy of the system.

The only distinction made between Ag^+ and Br^- ions was in the allowed distances, r_{i-j}, of closest approach. r_{Ag-Ag} and r_{Ag-Br} were set equal to the low-r cut-off in $G_e(r)$, 2.2 Å (see figure 2). $r_{Br-Br} = 3.4$ Å was estimated from the known Br^- diameter (3.92 Å) and the second peak in $G_e(r)$ (the first Br–Br peak). To ensure cubic lattice periodicity within the periodic boundary conditions the sides of the configuration cell L were such that $L = na$ where n is an integer and a is the unit cell parameter calculated from the Bragg peaks in $F(Q)$ at each temperature. The initial configuration used in the analysis of the lowest temperature data was the $T = 0K$ FCC crystal lattice. At higher temperatures a configuration determined from the data at the next lower temperature was used as a starting point (with a suitable change in the number density). In a previous paper (Keen *et al* 1989) 32 768 ions ($L = 16a$) were used in the simulation. It was found however that for the physical properties of interest (i.e. those related to the disorder in the system), such a large box was unnecessary and a 4096-ion ($L = 8a$) configuration was sufficient. The statistics on the results from this configuration were not as good, so eight statistically independent configurations were collected for each temperature. To ensure independence at least five moves per ion (i.e. >20 000 moves) were made between each saved configuration. Using these smaller configurations significantly sped up computation; $G_c(r)$ was converged to within 1% of $G_e(r)$ and then eight independent 4096-ion configurations were collected in 13 CPU hours using a Convex vector processor. Figure 2 shows radial distribution functions $G_e(r)$ from experimental data at $T = 490$ K and $T = 699$ K, in comparison with the calculated $G_c(r)$ averaged over the eight configurations.

At 293 K there are still large oscillations in $F(Q)$ at the maximum Q-value measured (figure 1) and these produced significant truncation ripples during the transform to $G(r)$. These ripples could be minimised by adding an artificial extension to $F(Q)$ before transformation. However it was found that some structural features were dependent on the choice of extension and hence the 293 K spectrum was not analysed further. A similar extension but with a much smaller amplitude was used prior to transformation of the

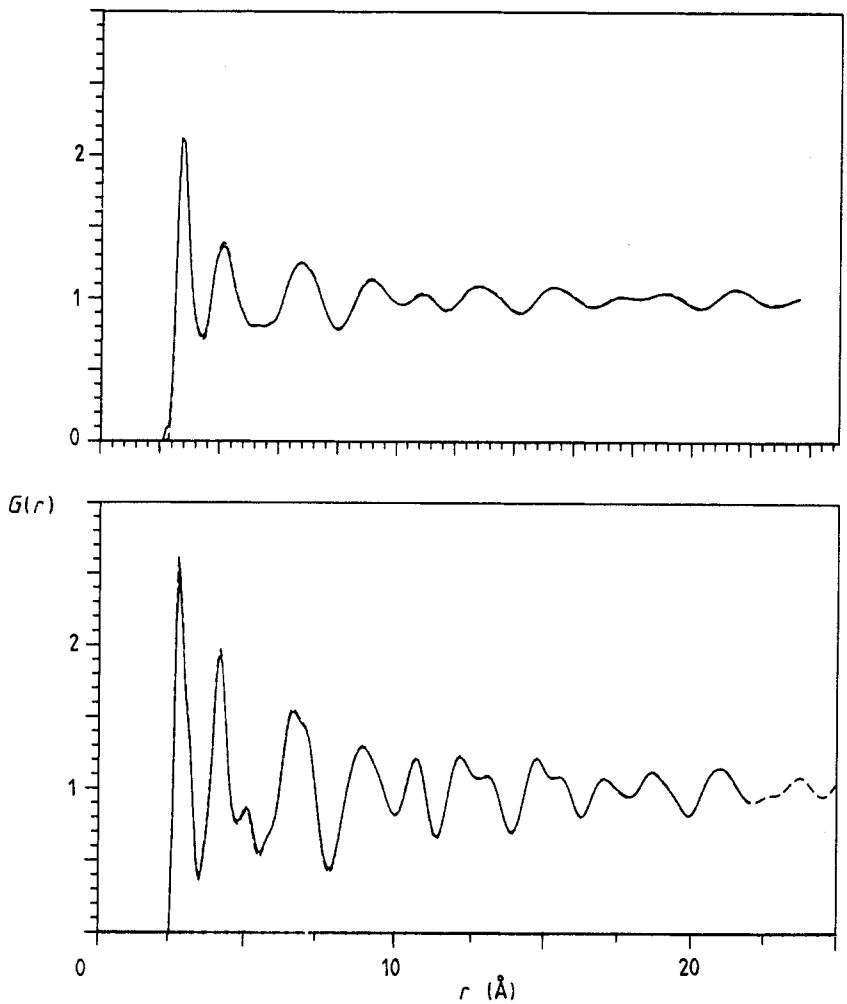

Figure 2. Total radial distribution functions $G(r)$ at (*a*) $T = 490$ and (*b*) $T = 699$ K. Broken curve, transform of the experimental data; full curve, RMC calculation.

490 K data; this only slightly affected the results obtained. No such extension was required for the higher temperature data sets. Measurements out to higher Q-values, possible on a pulsed neutron source, would alleviate this problem.

The spectrum for molten AgBr at 703 K was analysed under the same conditions as the solid discussed above, i.e. 4096 ions in a cubic cell with L chosen to correspond to the density of the melt and starting from the highest temperature crystal configuration (699 K). It was found that the Ag^+ ion distribution became liquid-like, but the Br^- ion distribution, though highly disordered, retained the crystal symmetry ('lattice' melt). σ_e was then set to ∞, so that the experimental data is effectively ignored and RMC is equivalent to a standard Monte Carlo simulation for (non-additive) hard spheres with diameters $r_{Ag\text{-}Ag} = r_{Ag\text{-}Br} = 2.2$ Å and $r_{Br\text{-}Br} = 3.4$ Å. The Ag^+ ion distribution became almost structureless (gas-like) and the Br^- ion distribution became even more disordered but was still crystalline. Evidently for the given density the hard-sphere system is slightly

below the melting point for the FCC crystal structure. However by decreasing r_{Br-Br} by 0.1 Å, to 3.3 Å, melting of the hard-sphere system was achieved; σ_e was then reset to its original value and the melt configuration was converged from this point, with no residual lattice symmetry in the Br^- distribution ('real' melt). Both 'real' and 'lattice' melts have similar short range order, and only differ significantly in terms of long range order. Note that there is no evidence suggesting a reduction in r_{Br-Br} in the crystal configurations. Measurements on other molten salts (see e.g. McGreevy 1987) show that ionic closest approaches often decrease slightly upon melting, even though the average ionic separation increases.

4. Results

The average density distribution of ions in the cubic unit cell has been produced by averaging the atomic positions over all the enclosed unit cells in eight configurations at each temperature. This is shown, projected onto the (100) plane, in figure 3 for four temperatures. The Br^- ion density around anion lattice sites remains approximately isotropic as temperature increases, with only a slight broadening. The situation for Ag^+ ion density around cation sites is quite different. The distribution is very anisotropic and the occupation of the $(\frac{1}{4}, \frac{1}{4}, \frac{1}{4})$ interstitial site becomes significant as the temperature approaches T_m.

Figures 1 to 3 give qualitative information about the disordering of Ag^+ ions. However the configurations can give quantitative information that would be impossible to obtain by inspection of the structure factors, especially when there are only subtle differences between the spectra at high temperatures (figure 1). From the average unit cell density it is possible to calculate the density distribution of ions about lattice sites in any direction, and hence the anisotropic mean square displacements (MSD) of ions from lattice sites. The RMC technique produces a structure consistent with *both* Bragg *and* diffuse scattering and therefore it would be expected to produce more reliable values of MSDs for a highly disordered material than those obtained from, for example, Rietveld refinement (Rietveld 1966, 1967). The Rietveld method refines a structure using Bragg peaks only, and obtains MSDs (isotropic or anisotropic) from the Debye–Waller factors used in the refinement. It can be seen from figure 1 that there are only a few, weak Bragg peaks in $F(Q)$ at the higher temperatures and this, together with the high symmetry of the crystal structure, limits the number of parameters that may be refined by the Rietveld method. Any attempt to refine anisotropic MSDs would be very inaccurate. To obtain information about the disorder in a material the diffuse scattering is more significant than the Bragg scattering. Bragg peaks (elastic scattering) are produced by time-average, long-range order in the crystal; the Debye–Waller factors calculated from them using Rietveld refinement assume a Gaussian distribution about lattice sites (harmonic vibrations). Diffuse scattering is produced by deviations from such order and must be included in any analysis to reliably calculate MSDs. The RMC method uses the total $F(Q)$, related to a 'snap-shot' ($t = 0$) picture of the structure, and makes no assumption about the form of the ionic distribution; in fact the Ag^+ ion density (figure 3) is found to be very anisotropic and non-Gaussian about lattice sites (indicating anharmonic vibrations).

The MSD's have been calculated from the average unit cell density. These are shown as a function of temperature in figure 4 for Ag^+ ion density in the ⟨100⟩, ⟨110⟩ and ⟨111⟩ directions and for Br^- ion density in the ⟨100⟩ direction together with the Ag^+ and Br^- MSDs (isotropic) calculated from the Bragg peaks via Debye–Waller factors. The MSDs

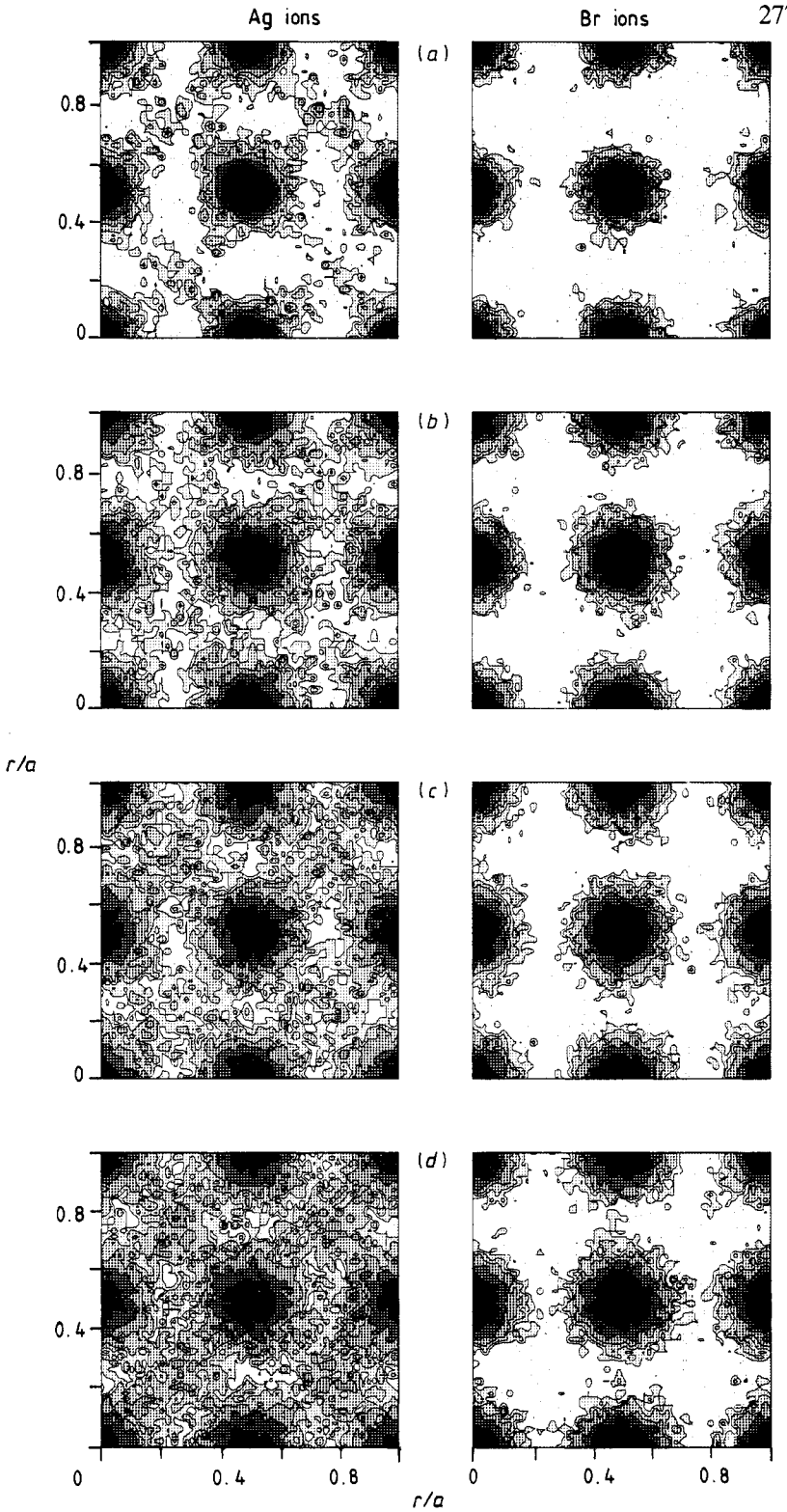

Figure 3. Density of Ag^+ and Br^- ions in the cubic unit cell projected onto the (100) plane. T = (*a*) 490, (*b*) 669, (*c*) 689 and (*d*) 699 K.

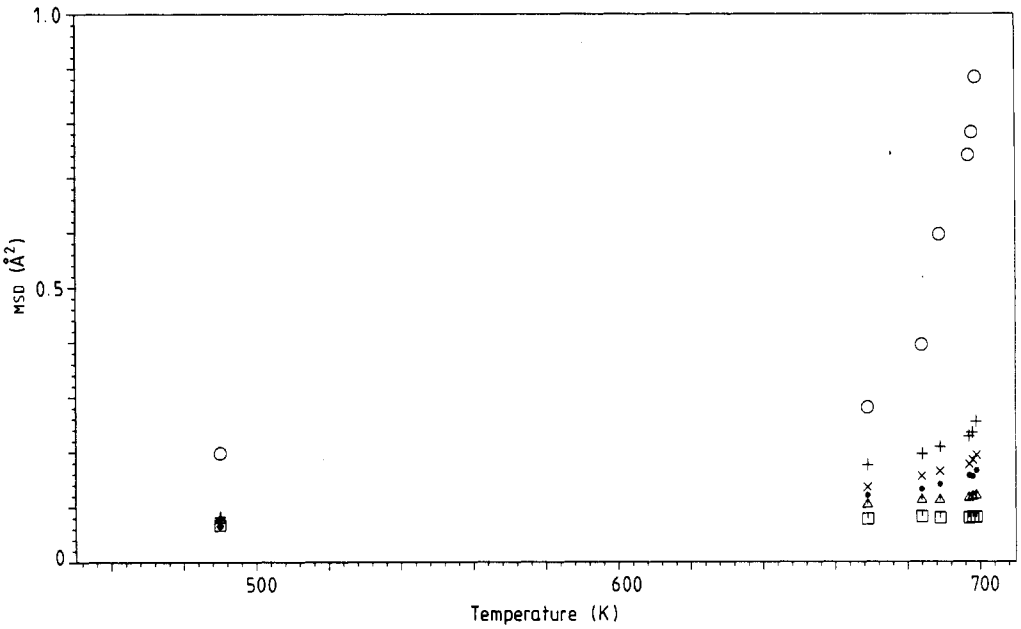

Figure 4. The mean squared displacement of ions about their lattice sites as a function of temperature; (○) Ag^+ in ⟨111⟩ directions, (+) Ag^+ in ⟨110⟩ directions, (×) Ag^+ in ⟨100⟩ directions and (●) Br^- in ⟨100⟩ directions calculated from the RMC generated configurations. (△) and (□) show the isotropic Ag^+ and Br^- values (divided by 3) calculated from the Bragg peaks only.

from the Debye–Waller factors are much smaller than those calculated from the configurations, since they take no account of the anharmonic vibrations that extend a long way from the lattice sites. There is little difference between the values in the three directions for the Br^- ion density. The MSDs only change slowly with temperature, except for that of Ag^+ ions in the ⟨111⟩ direction, which has a much higher value than in other directions at the lower temperatures and at temperatures close to T_m becomes anomalously large.

Figure 5 shows the density profile across the cation lattice site, out to half the distance between neighbouring cation lattice sites, in the ⟨100⟩, ⟨110⟩ and ⟨111⟩ directions for $T =$ 669 K. In all three directions the distribution is approximately Gaussian with the same width out to $r = 0.15a$, after which the distribution deviates from Gaussian in the ⟨111⟩ direction with a long 'tail' which is responsible for the anomalous behaviour of the MSD in this direction. The other interesting temperature dependent feature of the Ag^+ ion density in ⟨111⟩ directions is that, when $T_m - T < 15$ K, a small peak in density occurs at $r = \pm 0.43a$ (figure 6). This is the position of the $(\frac{1}{4}, \frac{1}{4}, \frac{1}{4})$ interstitial site.

For a density distribution where there is no region of zero density between the lattice site and the interstial position, any structural definition of the number of interstitials must be arbitrary. If the region which is counted as interstitial is too large then density is included which corresponds to Ag^+ ions undergoing anharmonic vibrations about the lattice site, and if the region is too small some real interstitial density may be omitted. However, by defining interstitial ions to be those ions within a chosen radius of the interstitial site, an interstitial occupancy may be calculated. Values obtained are shown for Ag^+ in table 1 using a radius of $0.12a$, which is slightly closer to the interstitial site

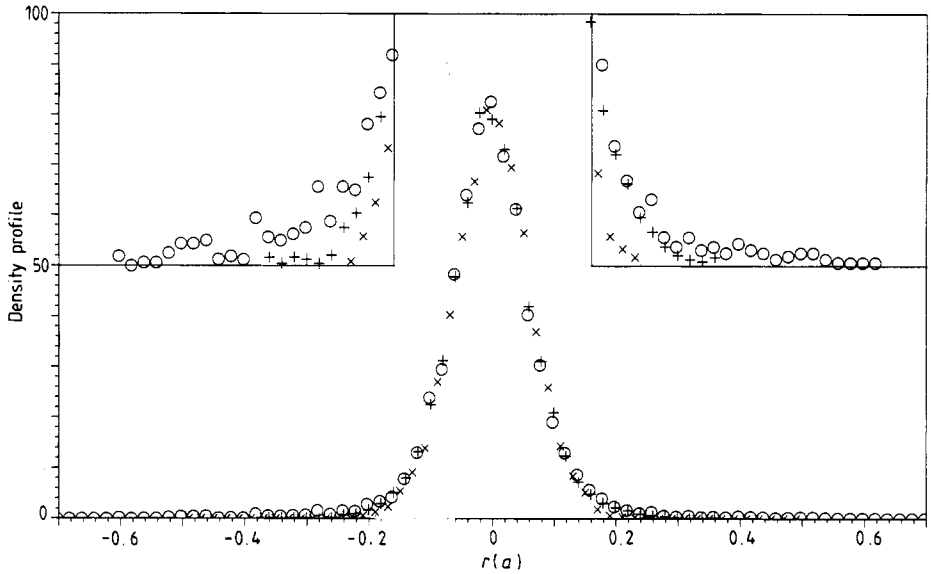

Figure 5. The density profile across Ag^+ lattice sites at 669 K in ⟨111⟩ directions (○), ⟨110⟩ directions (+) and ⟨100⟩ directions (×). The scale for the insets has been reduced by a factor of 10.

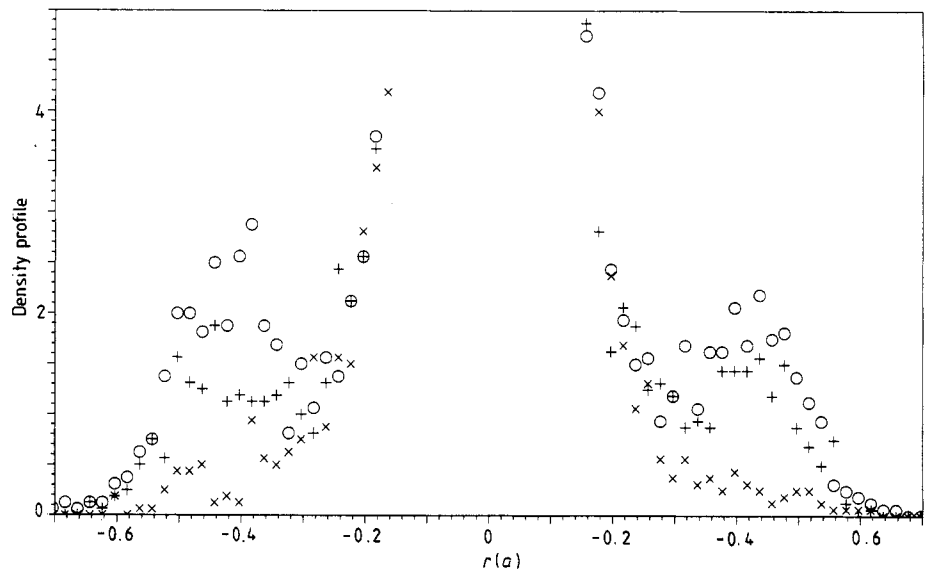

Figure 6. The density profile across Ag^+ lattice sites in ⟨111⟩ directions at $T = 669$ (×), 689 (+) and 699 K (○).

than the density minimum in figure 6. All other cations and anions which are not found to occupy interstitial sites may then be assigned to their closest cation and anion lattice sites respectively. Hence the occupancy of each lattice site may be estimated. Only one

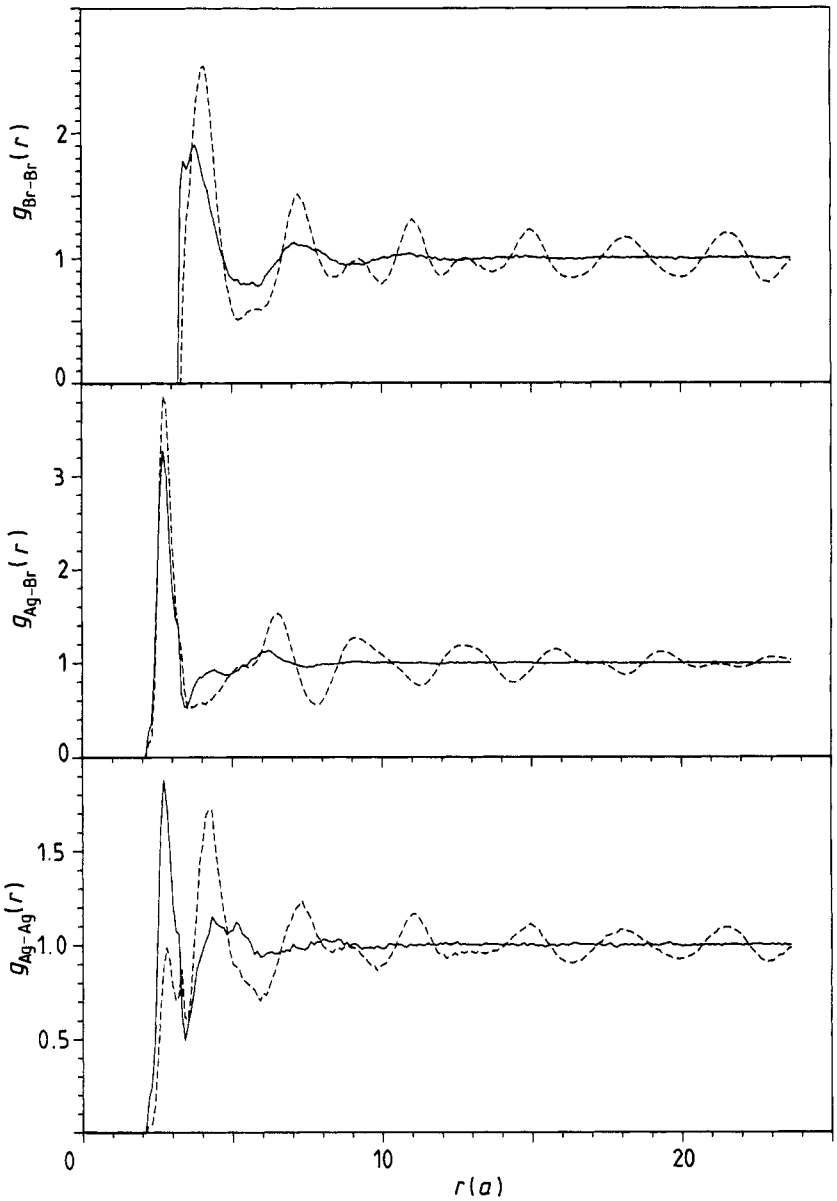

Figure 7. Partial radial distribution functions $g_{ij}(r)$ of the melt at $T = 703$ K (full trace) and the solid at $T = 699$ K (dotted trace).

interstitial Br^- ion was found in the eight configurations and then only at 699 K, and anion lattice sites are approximately singly occupied. The occupancy of cation lattice sites is shown in table 1. There are more vacant cation lattice sites than Ag^+ interstitials, because there are a number of multiply occupied cation lattice sites.

The partial radial distribution functions for the 'real' melt are shown in figure 7, in comparison with those for the solid at $T = 699$ K. It can be seen that the first peak in $g_{Ag-Ag}(r)$ in the melt occurs at a similar distance to the interstitial-lattice site separation

Table 1. The interstitial and lattice site occupancy of Ag^+ ions at a number of temperatures. The interstitial occupancy is given as the percentage of Ag^+ ions in interstitial sites as defined in the text, and the lattice site occupancy is the percentage of sites which are either vacant, singly or doubly occupied by Ag^+ ions. The lattice constant is also given for information.

			Lattice site occupancy (%)		
T (K)	a (Å)	Interstitial occupancy (%)	0	1	2
293	5.78 ± 0.01	—	—	—	—
490†	5.82 ± 0.01	1.8 ± 0.3	2.0 ± 0.4	97.9 ± 0.5	0.2 ± 0.1
669	5.90 ± 0.01	1.1 ± 0.2	1.7 ± 0.4	97.8 ± 0.7	0.5 ± 0.3
684	5.92 ± 0.01	1.9 ± 0.2	3.0 ± 0.6	96.0 ± 1.0	1.1 ± 0.5
689	5.92 ± 0.01	3.3 ± 0.4	5.1 ± 0.6	93.0 ± 0.9	1.9 ± 0.3
697	5.93 ± 0.01	4.3 ± 0.4	6.9 ± 0.5	90.5 ± 0.9	2.6 ± 0.4
698	5.94 ± 0.01	4.6 ± 0.2	8.2 ± 0.3	88.2 ± 0.5	3.5 ± 0.3
699	5.94 ± 0.01	5.0 ± 0.2	9.0 ± 0.1	87.1 ± 0.4	3.9 ± 0.2

† The occupancy values at this temperature are slightly inconsistent with the values at the other temperatures. These small errors are thought to have been introduced by artificially extending $F(Q)$ (see text).

in the crystal. Analysis of the bond angle distribution within the first like and unlike ion coordination shells (defined by the first minima in $g_{ij}(r)$) shows that the underlying local symmetry of Br^- in the melt is octahedral, as it is in the crystal. In the liquid the Ag^+ site in the centre of the Br^- octahedron is often vacant; however when it is occupied the nearest neighbour Ag^+ ions preferentially occupy sites in the direction of the faces of the Br^- octahedron, i.e. the 'interstitial' sites, rather than in the direction of the edges of the octahedron, i.e. 'lattice' sites.

5. Discussion

We shall limit our discussion of results to two main areas: firstly to what can be said about the ionic conduction process at elevated temperatures and secondly about the general disordering of the lattice that leads to melting.

5.1. Ionic conductivity

Aboagye and Friauf (1975) calculate from ionic conductivity measurements that there are nearly 2% of Ag^+ ions involved in conduction via interstitial sites for temperatures close to T_m. We obtain a much higher value of Ag^+ interstitial occupancy at $T = 699$ K (table 1). This difference occurs for a number of reasons, but principally because we have made an arbitrary, though reasonable, definition of a *structural* interstitial; this is simply defined as Ag^+ ions within a certain radius of the interstitial site. The number of interstitials is dependent on this radius; the larger its value the greater the interstitial occupancy. The density 'tails' due to anharmonic thermal vibrations in ⟨111⟩ directions from neighbouring cation lattice sites cannot be completely excluded using this definition. Since the interstitial-vacancy coordination number is very close to unity (i.e. nearly all interstitials have a nearest neighbour vacancy), many interstitials may be undergoing local motion about their nearest vacant lattice site and are not necessarily

involved in long range ionic conduction. It should also be noted that the interstitial occupancy derived from conductivity measurements is dependent on the model chosen to theoretically predict the conductivity. Aboagye and Friauf (1975) used an empirical temperature-dependent energy of Frenkel interstitial formation and assumed no structural disorder in their model. This assumption is obviously an oversimplification in the light of our results.

Five possible conduction mechanisms have been summarised by Hamilton (1988):

(a) Collinear interstitialcy jumps in which an interstitial Ag^+ ion replaces an Ag^+ ion on a neighbouring lattice site, displacing it to the opposite interstitial site;

(b) non-collinear interstitialcy jumps;

(c) direct interstitial jumps, e.g. from $(\frac{1}{4}, \frac{1}{4}, \frac{1}{4})$ to $(\frac{3}{4}, \frac{1}{4}, \frac{1}{4})$,

(d) direct vacancy jumps in which a lattice cation moves directly along $\langle 110 \rangle$ to a nearest neighbour cation vacancy, and

(e) a pair of non-collinear $\langle \frac{1}{4}, \frac{1}{4}, \frac{1}{4} \rangle$ jumps in which a lattice cation moves to an interstitial site and then relaxes to a different vacant lattice site.

On the basis of conductivity and self-diffusion measurements it is found that (a) predominates, (b) and (c) are observed and (d) and (e) are energetically unfavourable; also the vacancy has a very low mobility ($\mu_{\text{vacancy}} \simeq 10^{-4}\, \mu_{\text{interstitial}}$ for Ag^+ ions at room temperature) (Hamilton 1988).

Since we have made neutron diffraction measurements, the configuration that we have calculated is only a 'snap-shot' picture of the structure and does not contain any direct dynamical information. However it is nevertheless possible to look for features of the static ionic distribution that might characterise the above dynamic mechanisms of ionic conduction. Below 669 K the average density distribution in the unit cell shows that neighbouring cation lattice sites are only connected by non-zero density via the interstitial site (i.e. $000 \rightarrow \frac{111}{444} \rightarrow \frac{1}{2}\frac{1}{2}0$, mechanisms (a), (b) or (e)). Above 669 K there is also non-zero density joining the cation lattice sites directly ($000 \rightarrow \frac{1}{2}\frac{1}{2}0$, mechanism (d)). Above 669 K the lowest value of the density along the route via the interstitial site is $\simeq$ 10 times larger than the lowest value of the density along the direct route. For $T \geq 697$ K the pathway of the direct interstitial jump (mechanism (c)) also has non-zero density everywhere, with a minimum value $\simeq$4 times smaller than that of the route via the interstitial site. These density values have relevance to the relative likelihood of ionic conductivity via the different pathways through the lattice and suggest that below 669 K only mechanisms (a), (b) and (e) are important. As the temperature rises more pathways are allowed, although mechanisms (a), (b) and (e) appear to be still more likely than (c) and (d) at 699 K. Table 1 shows a significant number of doubly occupied cation lattice sites. These could be considered as an intermediate stage of mechanisms (a) and (b). The ion–lattice-site–ion angular distribution of these doubly occupied sites shows that the preferred angle is close to 180°, rather than 90°, which suggests that mechanism (a) predominates over (b). Mechanism (e) is extremely unlikely since an intermediate stage of this process would be two cation lattice vacancies near an interstitial Ag^+ ion but, as already stated, the interstitial–vacancy coordination is very close to unity.

These results are therefore entirely consistent with transport measurements. Information on Ag^+ ion motion could be obtained from single crystal inelastic neutron scattering measurements, though analysis of such data is also indirect and relies on some form of model. Molecular dynamics simulation can be used to obtain direct information, but this is then dependent on the choice of interatomic potentials.

It is instructive at this stage to compare AgBr and AgI. Although the conductivity in AgI just below the melting point is only three times as large as that in AgBr all of the Ag^+ ions in AgI may be considered as carriers, compared to <5% in AgBr. The Ag^+ ion mobility in AgBr must therefore be significantly higher than in AgI. Inelastic neutron scattering experiments (Eckold *et al* 1976) show that the low energy scattering, which gives rise to the thermal diffuse scattering in $F(Q)$, is predominantly quasi-elastic in AgI and the conduction process is dominated by thermally activated hopping of Ag^+ ions between possible lattice sites (in the tetrahedral model there are 12 sites for 2 Ag^+ ions). Inelastic neutron scattering measurements on AgBr (to be reported in a later paper) show little quasi-elastic scattering but, rather, scattering by low energy phonons whose intensity increases anomalously with temperature. The large differences in both mobility and low energy scattering between AgI and AgBr suggest some form of 'collective' conductivity mechanism in AgBr.

5.2. *Melting*

Lindemann (1910) suggested that when the vibrational amplitude of atoms in a solid became greater than $\simeq 0.1$ of the interatomic spacing then the lattice would become unstable and melt. 0.1 of the interatomic separation in AgBr at 699 K is 0.3 Å. The half-width at half-height (HWHH) of the density distribution about lattice sites should be a good approximation fo the amplitude of vibration. At 699 K this is 0.44 Å for Br^- ions and 0.47 Å for Ag^+ ions, larger than the Lindemann criterion; this is true for all the temperatures measured. If one used the root mean square displacement (equal to the HWHH for a Gaussian distribution) then the discrepancy would be even larger. However this is not particularly surprising, since the Lindemann criterion is only really applicable to harmonic systems, and it is clear that the vibrations in AgBr are highly anharmonic.

The local structure of the melt, discussed previously, is clearly a 'continuation' of the disordering process occurring in the crystal. At low temperatures in the FCC crystal structure a Ag^+ ion is octahedrally coordinated by Br^- ions, and then has twelve Ag^+ neighbours in the same direction as the *edges* of the Br− octahedron. As the temperature increases Ag^+ ions gradually occupy interstitial $(\frac{1}{4}, \frac{1}{4}, \frac{1}{4})$ sites which are approximately in the direction of the *faces* of the Br^- octahedron. In the melt the octahedral Br^- coordination remains, though considerably disordered, and neighbouring Ag^+ ions occupy the face (interstitial) sites. It is not yet clear how much more the Ag^+ sub-lattice disorders before melting; to determine this similar measurements are planned much closer to T_m.

6. Conclusions

We have shown that information about the ionic disorder that occurs during premelting in AgBr can be obtained by RMC analysis of powder neutron diffraction data. The mean squared displacement of Ag^+ ions about cation lattice sites is largest in the ⟨111⟩ directions and increases anomalously at temperatures close to T_m. A small peak in density is observed at the $(\frac{1}{4}, \frac{1}{4}, \frac{1}{4})$ interstitial site for $T_m - T < 15$ K. The ionic distribution is consistent with the mechanisms used to explain ionic conductivity data; at lower temperatures the only mechanism is the collinear interstitialcy jump while at higher temperatures other mechanisms are possible, although the collinear interstitialcy jump

still dominates. The local structure in molten AgBr shows features similar to the disorder in the solid.

Acknowledgments

We wish to thank the staff of the Institut Laue–Langevin, in particular Pierre Convert, for assistance with these experiments. RLM thanks the Royal Society for continued support.

References

Aboagye J K and Friauf R J 1975 *Phys. Rev.* B **11** 1654
Andreoni W and Tosi M P 1983 *Solid State Ion.* **11** 49
Batra A P and Slifkin L M 1976 *J. Phys. C: Solid State Phys.* **9** 947
Börjesson L and Torell L M 1987 *Phys. Rev.* B **36** 4915
Boyce J B and Huberman B A 1979 *Phys. Rep.* **51** 189
Devlin B A and Corish J 1987 *J. Phys. C: Solid State Phys.* **20** 705
Eckold G, Funke K, Kalus J and Lechner R E 1976 *J. Phys. Chem. Solids* **37** 1097
Friauf R J 1984 *The Physics of Latent Image Formation in Silver Halides* ed A Baldereschi *et al* (Singapore: World Scientific) p 79
Hamilton J F 1988 *Adv. Phys.* **37** 359
Hayes W 1978 *Contemp. Phys.* **19** 468
—— 1986 *Contemp. Phys.* **27** 519
Howe M A, McGreevy R L and Mitchell E W J 1985 *Z Phys.* B **62** 15
Keen D A, McGreevy R L, Hayes W and Clausen K N 1990 *Phil. Mag. Lett.* submitted
Lawn B R 1963 *Acta Crystallogr.* **16** 1163
Lindemann F A 1910 *Phys. Z. Sowjun.* **14** 609
McGreevy R L 1987 *Solid State Phys.* **40** 247
McGreevy R L and Pusztai L 1988 *Mol. Simul.* **1** 359
Mellander B-E and Lazarus D 1984 *Phys. Rev.* B **29** 2148
Metropolis N, Rosenbluth A W, Rosenbluth M N, Teller A H and Teller E 1953 *J. Chem. Phys.* **21** 1087
Reitveld H M 1966 *Acta Crystallogr.* **20** 258
—— 1967 *Acta Crystallogr.* **22** 151